

Structural and dynamical heterogeneities in two-dimensional melting

HAYATO SHIBA, AKIRA ONUKI and TAKEAKI ARAKI

Department of Physics, Kyoto University, Kyoto 606-8502, Japan

PACS 64.70.D- – Solid-liquid transitions
PACS 61.72.J- – Point defects and defect clusters
PACS 83.10.Rs – Computer simulation of molecular and particle dynamics

Abstract. - Using molecular dynamics simulation, we study structural and dynamical heterogeneities at melting in two-dimensional one-component systems with 36000 particles. Between crystal and liquid we find intermediate hexatic states, where the density fluctuations are enhanced at small wave number k as well as those of the six-fold orientational order parameter. Their structure factors both grow up to the smallest wave number equal to the inverse system length. The intermediate scattering function of the density $S(k, t)$ is found to relax exponentially with decay rate $\Gamma_k \propto k^z$ with $z \sim 2.6$ at small k in the hexatic phase.

Introduction. – Since a simulation by Alder and Wainwright [1], much attention has been paid to the two-dimensional (2D) melting in simple one component particle systems [2]. However, it has been controversial whether the transition is first order as in three-dimensional melting [1–5] or is continuous as predicted by Halperin and Nelson [6]. They presented a defect-mediated melting mechanism and a “hexatic phase” in a temperature (or density) window between crystal and liquid. In the hexatic phase, the bond-orientation correlation function $g_6(r)$ of a sixfold orientation order parameter $\psi_6(\mathbf{r})$ decays algebraically, indicating a quasi-long-range orientational correlation. Afterwards their prediction has been confirmed in experiments [7–12] and in simulations [13–20]. In the hexatic phase, defects have been observed to proliferate with increasing the temperature T or decreasing the density n . As other theories, Chui proposed a melting mechanism mediated by grain boundaries [21], while Saito argued that the 2D melting can be either continuous or first order depending on the specific details of the system [15].

As a marked feature, a number of experiments and simulations [1–3, 7–14, 22] have observed heterogeneities in the hexagonal structures and in the particle trajectories, developing around the transition. In particular, appreciable dependence on the system size has been encountered in the calculations of the equation of state [1, 5, 17, 20] and the local fluctuations of $\psi_6(\mathbf{r})$ [5, 20]. However, the heterogeneities in the 2D melting have not yet been well understood. In this Letter, we will visualize them using a

disorder variable representing deviations from the hexagonal order [23] and bond breakage used in analyzing glass dynamics [24]. It is also a fundamental issue whether the isothermal compressibility $K_T = (\partial n / \partial p)_T / n$ remains finite or tends to infinity in the hexatic phase. In simulations [17, 20], the pressure p was a weakly decreasing function of n , apparently suggesting $(\partial p / \partial n)_T < 0$, in the hexatic phase. Hence, we will calculate the structure factor of the density $S(k)$ at small wave number k to see whether the thermodynamic relation $\lim_{k \rightarrow 0} S(k) = n^2 T K_T$ holds or not. The intermediate scattering function $S(k, t)$ will then emerge as a new informative quantity.

Numerical Method. – Our 2D system is composed of $N = 36000$ particles interacting via a truncated Lennard-Jones potential of the form

$$v(r) = 4\epsilon [(\sigma/r)^{12} - (\sigma/r)^6] - C, \quad (1)$$

which is characterized by the energy ϵ and the range σ . For $r > r_{\text{cut}} = 3.2\sigma$, we set $v(r) = 0$ with the constant C ensuring the continuity of $v(r)$ at the cut-off. The system volume V is kept fixed such that $\phi = N\sigma^2/V = 0.9$. Then the system length is given by $L = V^{1/2} = 200\sigma$. We integrated the equations of motion using the Störmer-Verlet algorithm (a sort of the leap-frog method) under the periodic boundary conditions using the Nosé-Hoover thermostat. The time step of integration is 0.002τ with

$$\tau = \sigma \sqrt{m/\epsilon}, \quad (2)$$

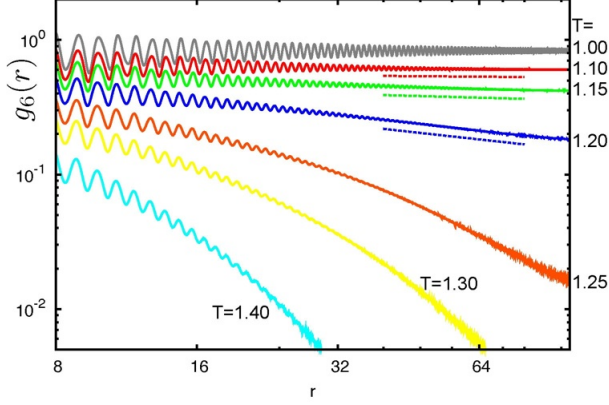


Fig. 1: Bond-orientational correlation function $g_6(r)$ on a logarithmic scale for $T = 1.0, 1.1, 1.15, 1.2, 1.25, 1.3$, and 1.4 from above, obtained from data averaged over long-time and over runs starting with 5 independent initial conditions. Below the curves of $T = 1.1, 1.15$, and 1.2 , dotted line segments are guides to eye with slopes $-0.03, -0.09$, and -0.36 , respectively.

m being the particle mass. In our simulations, we first quenched the system from $T = 2\epsilon/k_B$ to $0.2\epsilon/k_B$ into a crystal state. After a relaxation time of $5 \times 10^3 \tau$, there was no appreciable time evolution in physical quantities such as the pressure and $g_6(r)$. We then increased T to a desired value. The time t is set equal to 0 at this temperature increase. We continued the simulation until $t = 2 \times 10^4 \tau$. Hereafter we will measure space, time, and T in units of σ , τ , and ϵ/k_B , respectively.

In 2D dense particle systems, a large fraction of the particles are enclosed by six particles and the local order is represented by the sixfold orientation [6]. We define the orientation angle α_j in the range $[-\pi/6, \pi/6]$ for each particle j at position \mathbf{r}_j using the complex number

$$\Psi_j = \sum_{k \in \text{bonded}} \exp[6i\theta_{jk}] = |\Psi_j| e^{6i\alpha_j}, \quad (3)$$

where the summation is over particles “bonded” to the particle j . The two particles j and k are bonded if $|\mathbf{r}_j - \mathbf{r}_k| \leq 1.25\sigma$. θ_{jk} is the angle between $\mathbf{r}_j - \mathbf{r}_k$ and the x axis [23, 24]. Next we construct another nonnegative-definite variable representing the degree of disorder for each particle j by [23]

$$D_j = 2 \sum_{k \in \text{bonded}} [1 - \cos 6(\alpha_j - \alpha_k)]. \quad (4)$$

Here D_j is nearly zero for a perfect crystal, but is large in the range 5 – 20 for particles around defects. Thus D_j is convenient in visualizing the structural inhomogeneity.

In terms of α_j the sixfold orientation order parameter $\psi_6(\mathbf{r})$ is defined as [6]

$$\psi_6(\mathbf{r}) \equiv \sum_{j=1}^N e^{6i\alpha_j} \delta(\mathbf{r} - \mathbf{r}_j). \quad (5)$$

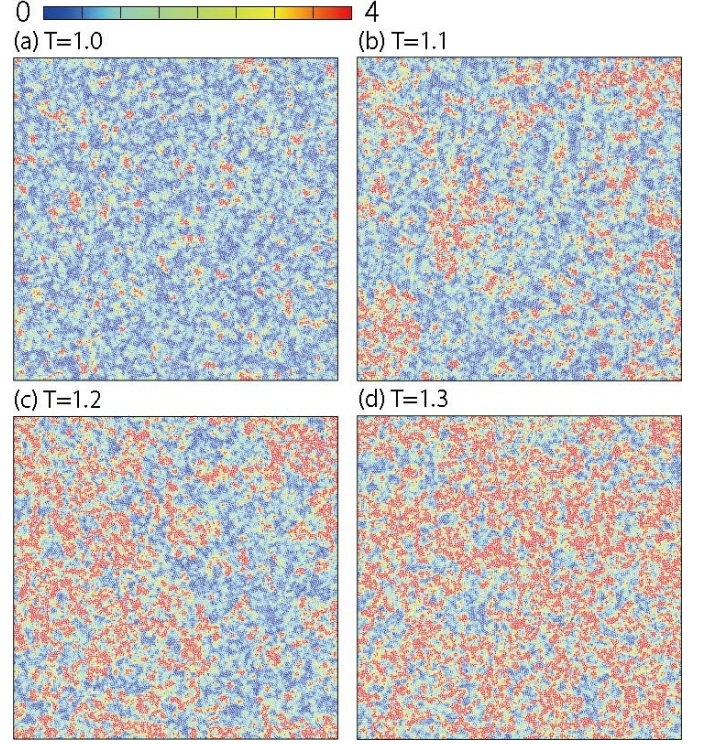


Fig. 2: Snapshots of disorder variable D_j of 36000 particles at $t = 1.2 \times 10^4$ for (a) $T = 1.0$ (crystal), (b) $T = 1.1$ (hexatic), (c) $T = 1.2$ (hexatic), and (d) $T = 1.3$ (liquid). Colors are given according to the bar on the top. Particles with $D_j > 4$ are written in red.

In the hexatic phase, the bond-orientational correlation function decays algebraically as

$$g_6(r) = \langle \psi_6(\mathbf{r}) \psi_6(\mathbf{0})^* \rangle \sim r^{-\eta}, \quad (6)$$

where $r = |\mathbf{r}|$. Theoretically [6], the exponent η depends on T and $n = N/V$ in the range $0 < \eta < 1/4$.

Structural Heterogeneity. – In fig. 1, the curves of $g_6(r)$ are displayed, which are the long-time averages over the snapshots produced by 5 independent runs in the range $10^4 < t < 2 \times 10^4$. In the hexatic phase at $T = 1.1, 1.15$, and 1.2 , the exponent η in eq. (6) is 0.03, 0.09, and 0.36, respectively, where 0.03 at $T = 1.1$ is very small and 0.36 at $T = 1.2$ even exceeds the theoretical upper bound $1/4$. The hexatic-liquid and crystal-hexatic transitions are continuous, taking place at $T \cong 1.2$ and 1.0 respectively. For our system size, it is still difficult to determine the transition temperatures precisely. For $T \geq 1.25$ the system is in liquid with $g_6(r)$ decaying exponentially, while for $T \leq 1.0$ the system is in crystal without appreciable decay of $g_6(r)$.

In fig. 2, we display snapshots of D_j of all the particles in a crystal phase at $T = 1.0$ (a), in hexatic phases at $T = 1.1$ (b) and 1.2 (c), and in a liquid phase at $T = 1.3$ (d). In fig. 3 (a), a more expanded snapshot

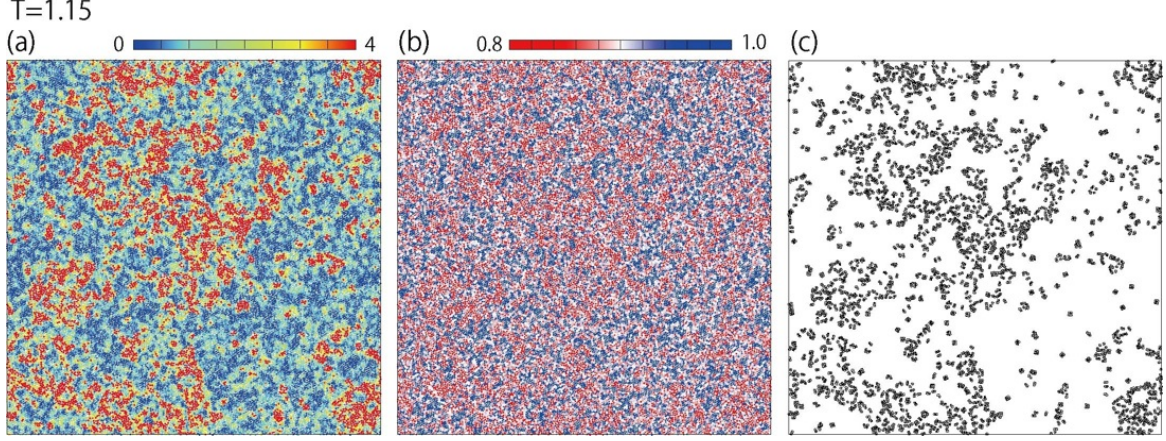


Fig. 3: Snapshot of disorder variable D_j (a), local packing density ρ_j (b), and particles with neighbor number different from six (c) for 36000 particles at $T = 1.15$. These three panels exhibit heterogeneous patterns stemming from the same long-range structural disorder.

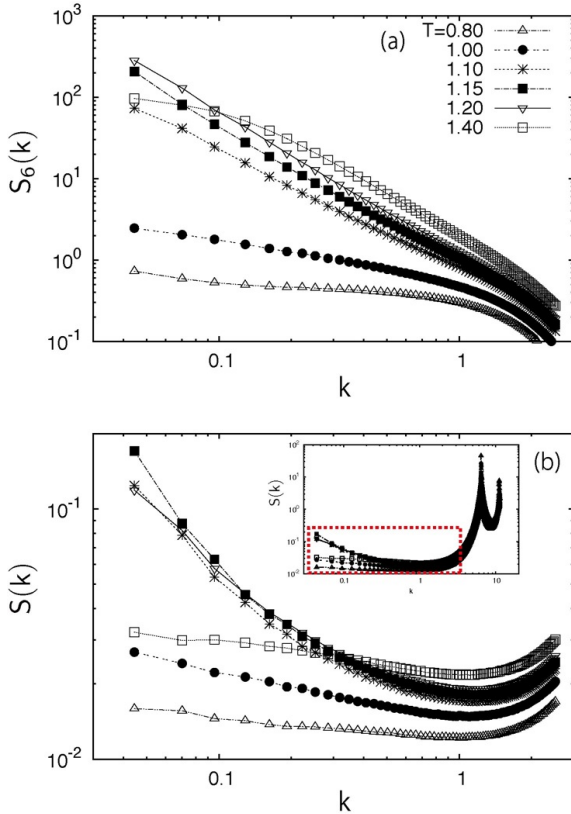


Fig. 4: Structure factors (a) $S_6(k)$ and (b) $S(k)$ for the six-fold orientation order and the density, respectively, for $T = 0.8, 1.0, 1.1, 1.15, 1.2$, and 1.4 , calculated as the long-time average. Averages are taken also over 5 independent runs. Use of mark in (b) is similar to (a). They are enhanced at long wavelengths in the hexatic phase.

of D_j is given at $T = 1.15$. The average disorder parameter $\bar{D} \equiv \sum_j D_j / N$ is 1.07, 1.72, 2.12, 2.55, and 3.32 for $T = 1.0, 1.1, 1.15, 1.2$ and 1.3 respectively. In the hexatic phases ($1.1 \leq T \leq 1.2$), marked heterogeneity emerges on large scales among crystalline and disordered regions, though there are no sharp boundaries. The patterns are fractal-like, resembling the critical fluctuations near the Ising criticality. Also shown in fig. 3 are (b) the local areal density ρ_j (to be defined below) and (c) the particles with neighbor number being different from six. A common particle configuration was used for these three panels. Here $v_j = \rho_j^{-1}$ is the volume of particle j in the Voronoi cell construction. We treat its inverse ρ_j as the local density at the position of particle j . Its variance $\mathcal{V} (= \langle \sum_j (\rho_j - \bar{\rho})^2 / N \rangle)$ is about 0.05 with $\bar{\rho} = \sum_j \rho_j / N \cong 0.9$ here. Comparing the two panels we can see that the particles with larger D_j tend to have smaller ρ_j . In the literature [7, 10, 12], defects have been detected around the particles with five or seven neighbors, so we used this Voronoi method to produce fig. 3 (c). It exhibits essentially the same heterogeneity as that of D_j (a), though only discrete particles are selected. However, near melting, using D_j is more quantitative and appropriate to characterize the diffuse disordered regions extending on large scales.

The algebraic decay of $g_6(r)$ in eq.(4) arises from the heterogeneity in figs. 2 and 3. Furthermore, fig. 3 (b) indicates that small density differences exist among the crystalline and disordered regions. In fig. 4, we thus show the structure factors of the hexagonal order and the density

$$S_6(k) = \int d\mathbf{r} e^{i\mathbf{k} \cdot \mathbf{r}} g_6(r) = \langle |\psi_{6\mathbf{k}}|^2 \rangle, \quad (7)$$

$$S(k) = \int d\mathbf{r} e^{i\mathbf{k} \cdot \mathbf{r}} \langle \delta \hat{n}(\mathbf{r}) \delta \hat{n}(\mathbf{0}) \rangle = \langle |\hat{n}_{\mathbf{k}}|^2 \rangle, \quad (8)$$

where $\delta \hat{n}(\mathbf{r}) = \sum_j \delta(\mathbf{r} - \mathbf{r}_j) - n$ is the microscopic density deviation. The $\psi_{6\mathbf{k}}$ and $\hat{n}_{\mathbf{k}}$ are the Fourier components of

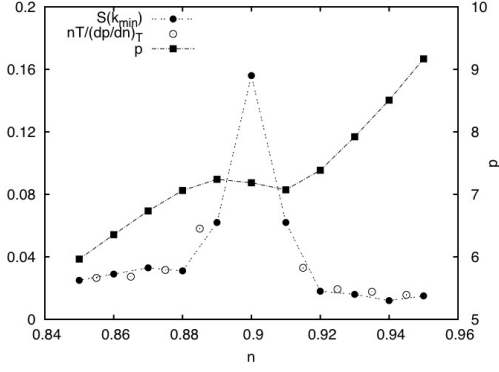


Fig. 5: Pressure p (right axis) vs density n at $T = 1.15$ with a small negative slope in the hexatic phase. Compared are resultant $nT/(\partial p/\partial n)_T$ and $S(k_{\min})$ (left axis), which coincide outside the hexatic region confirming the compressibility relation. In the hexatic phase, $(\partial p/\partial n)_T$ is apparently negative and the long wavelength limit $S(0)$ is not attained for our system size.

$\psi_6(\mathbf{r})$ and $\hat{n}(\mathbf{r})$. These structure factors are the averages over the angle of the wave vector $\mathbf{k} = (k_x, k_y)$. The smallest wave number k_{\min} is defined as $\pi(1 + \sqrt{2})/L = 0.035$, where $L = 200$ is the system length. The structure factors at $k = k_{\min}$ are the averages of the data at $\mathbf{k} = 2\pi L^{-1}(\pm 1, \pm 1)$ and $2\pi L^{-1}(\pm\sqrt{2}, \pm\sqrt{2})$. In fig. 4(a), the growth $S_6(k) \cong A_6 k^{-2+\eta}$ can be seen at small k in the hexatic phase at $T = 1.1, 1.15$, and 1.2 in accord with eq. (6), where $A_6 = 0.53$ and $\eta = 0.09$ at $T = 1.15$. In fig. 4 (b), $S(k)$ grows at small k in the hexatic phase, but its amplitude is very small and $S(k_{\min})$ remains smaller than the peak height at $k \sim 2\pi$ by two orders of magnitude (see the inset). In fact, at $T = 1.15$, its curve may be fitted to $S(k) \cong 0.017 + 1.23 \times 10^{-3}/k^{1.55}$ for $k < 1$. The small coefficient ($\sim 10^{-3}$) here arises from small density differences among the crystalline and disordered regions. For our system size, these structure factors do not saturate even at $k = k_{\min}$ in the hexatic phase.

If $S(k)$ saturates to a long wavelength limit $S(0) = \lim_{k \rightarrow 0} S(k)$ in the thermodynamic limit $L \rightarrow \infty$ at fixed density, the compressibility is given by $K_T = (\partial n/\partial p)_T/n = S(0)/n^2 T$. From our simulation only, however, we cannot exclude the possibility of $S(k) \rightarrow \infty$ (as $k \rightarrow 0$) in the hexatic phase, where $(\partial p/\partial n)_T = 0$ ultimately holds in the thermodynamic limit. As in fig. 5, we also performed simulations with 36000 particles by varying the volume V , where shown is the pressure p (average of its microscopic expression) vs the density n at $T = 1.15$. Outside the hexatic region, the long wavelength limit $S(0)$ is attained and the compressibility relation $S(0) = nT/(\partial p/\partial n)_T$ surely holds. Here, as in previous work [20], p apparently exhibits a small negative slope in the hexatic density range. Thus we need to use much larger system sizes to settle this issue. In such simulations, the long wavelength fluctuations (with $k < 10^{-2}$) need to

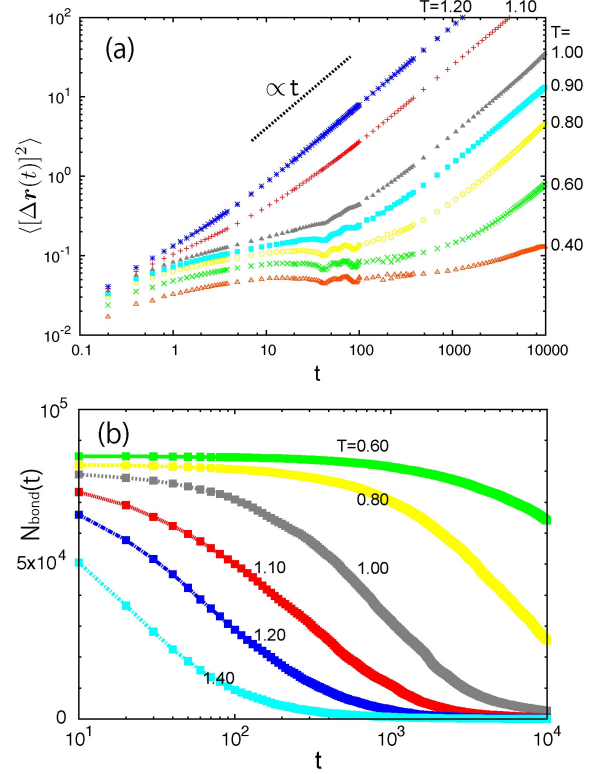


Fig. 6: (a) Mean-square displacement vs t for various T on a logarithmic scale, yielding the diffusion constant D_s . In crystal at $T = 0.6$ and 0.8 , its linear increase after a plateau is due to defect motion. (b) Surviving-bond number $N_b(t)$ vs t on a semi-logarithmic scale, decaying as e^{-t/τ_b} . Here $D_s \sim 1/\tau_b$.

be equilibrated on extremely long times.

Dynamics. – The dynamics has not yet been well studied at the 2D melting. For the particle displacement $\Delta \mathbf{r}_j(t) = \mathbf{r}_j(t + t_0) - \mathbf{r}_j(t_0)$ in time interval t , fig. 6 (a) displays the mean square displacement, $\langle [\Delta \mathbf{r}(t)]^2 \rangle = \sum_j \langle [\Delta \mathbf{r}_j(t)]^2 \rangle / N$, which is the average over all the particles and over the simulation time. The linear behavior $\langle [\Delta \mathbf{r}(t)]^2 \rangle \cong 4D_s t$ can be seen at long times for $T \geq 0.6$. The diffusion constant D_s thus obtained increases as 0.181, 1.13, 3.32, 8.23, 60.5, and 188 for $T = 0.6, 0.8, 0.9, 1, 1.1$, and 1.2 , respectively, in units of $10^{-4}\sigma^{-2}\tau^{-1}$. In crystal ($0.6 \leq T \leq 1.0$), the curves exhibit a plateau followed by the linear growth. Similar two-step behavior is well-known in supercooled liquids [24], but it is here due to motions of defect clusters composed of several particles with finite D_j (see fig. 2 (a)). Such clusters were observed in 2D colloidal systems [12]. In the hexatic phase, on the other hand, the plateau disappears and D_s grows abruptly.

To examine the particle-configuration changes, we introduce the bond breakage [24]. For each particle configuration at a time $t_0 (\sim 10^4)$ after long annealing, a pair of particles i and j is considered to be bonded if

$$r_{ij}(t_0) = |\mathbf{r}_i(t_0) - \mathbf{r}_j(t_0)| \leq A_1, \quad (9)$$

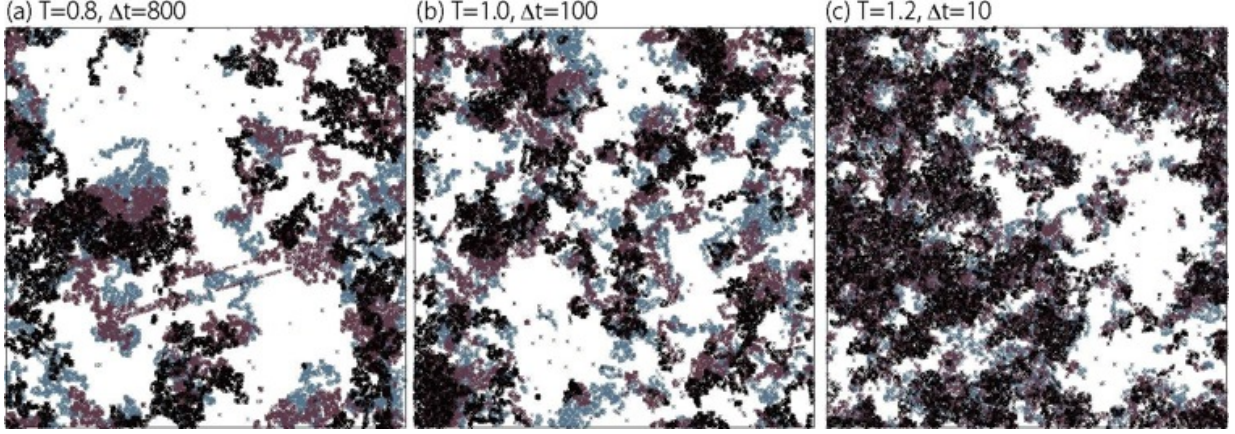


Fig. 7: Snapshots of broken bonds in three consecutive time intervals $[t_0 + (\ell - 1)\Delta t, t_0 + \ell\Delta t]$ ($\ell = 1, 2, 3$) for (a) $\Delta t = 800$ at $T = 0.8$, (b) $\Delta t = 100$ at $T = 1.0$, and (c) $\Delta t = 10$ at $T = 1.2$. Colors: ultramarine ($\ell = 1$), magenta ($\ell = 2$), and black ($\ell = 3$) in the chronological order. Corresponding snapshots of D_j of (a) and (b) at $\ell = 3$ are shown in fig. 2 (b) and (c)

where we set $A_1 = 1.2$ (around the peak distance of the pair correlation function). After a time interval t , the bond is regarded to be broken if

$$r_{ij}(t_0 + t) \geq A_2, \quad (10)$$

where we set $A_2 = 1.6$. In fig. 6 (b), we plot the number of the surviving bonds $N_b(t)$ vs t for various T . It is equal to the initial bond number $N_b(0)$ ($\sim 8.4 \times 10^4$) minus the number of the broken bonds. It may fairly be fitted to the exponential form e^{-t/τ_b} . The bond life time τ_b is determined by $N_b(\tau_b) = N_b(0)/e$. Then $\tau_b = 91, 8.1, 1, 0.3$, and 0.09 for $T = 0.6, 0.8, 1$, and 1.2 , respectively, in units of $10^3\tau$. Here we notice that the product $D_s\tau_b$ is between 1 and 2, where D_s is the diffusion constant determined in fig. 6 (a). Thus

$$D_s \sim \tau_b^{-1}, \quad (11)$$

which demonstrates that the particle motions are caused by the configuration changes in our jammed states.

We examine how the dynamic heterogeneity evolves in time. In fig. 7, we pick up the particles with broken bonds in three consecutive time intervals and mark them in ultramarine, magenta, and black in this order. Here we set (a) $\Delta t = 800$ at $T = 0.8$, (b) $\Delta t = 100$ at $T = 1.0$, and (c) $\Delta t = 10$ at $T = 1.2$. In crystal (a), the evolution is due to the motions of defect clusters taking place in the form of string-like trajectories in each event. Such trajectories accumulate to form large-scale dynamic heterogeneity on long time scales, though the defect number is small at each time in crystal. This picture explains the two-step behavior of $\langle[\Delta\mathbf{r}(t)]^2\rangle$ in crystal in fig. 6 (a). In addition, two straight lines arising from dislocation gliding can be seen in (a), but such slip motions are rare in our system. In (b), the system is still in crystal, but the time scale of bond breakage is much faster. In the hexatic phase (c), the particles in the disordered regions are relatively mobile, while those in the crystalline regions are

nearly immobile. The mobility of the particles is strongly correlated to the disorder variable D_j visualized in fig. 2 (c). The dynamic heterogeneity can be seen over a rather broad temperature range around the melting, where the time scale changes dramatically [9, 12–14, 22, 23].

Since the large-scale density fluctuations are enhanced as in fig. 4 (b), we are interested in their relaxation. As shown in fig. 8, we calculated the total intermediate scattering function

$$S(k, t) = \int d\mathbf{r} e^{i\mathbf{k}\cdot\mathbf{r}} \langle \delta\hat{n}(\mathbf{r}, t) \delta\hat{n}(\mathbf{0}, 0) \rangle \quad (12)$$

in the hexatic phase at $T = 1.15$ where the initial value $S(k)$ is enhanced as in fig. 4 (b). In an early stage it undergoes an oscillatory decay arising from the acoustic propagation. We find that it then decays exponentially as

$$S(k, t) \cong S(k) A_k e^{-\Gamma_k t}, \quad (13)$$

for small $k \ll 1$. The amplitude A_k approaches unity and the decay rate behaves as $\Gamma_k \sim k^z$ with $z \sim 2.6$ for small k . The dotted lines in fig. 8 represent this exponential form, which are excellently fitted to the numerical data. This slow decay arises from the evolution of large-scale density heterogeneities produced by the structural fluctuations. In the hexatic phase, the diffusion constant depends on the wave number as $D_k \propto k^{z-2}$ if it is introduced by $D_k = \Gamma_k/k^2$. This is analogous to the thermal diffusion constant at the gas-liquid criticality, where $z = 3$ in three dimensions [26]. However, we cannot explain this exponential relaxation in the hexatic phase at present. In passing, we also calculated $S(k, t)$ in crystal and liquid outside the hexatic temperature window, where the density fluctuations are much suppressed at small k . There, the long wavelength relaxation of $S(k, t)$ is due to hydrodynamic thermal diffusion with $\Gamma_k \propto k^2$ for small k .

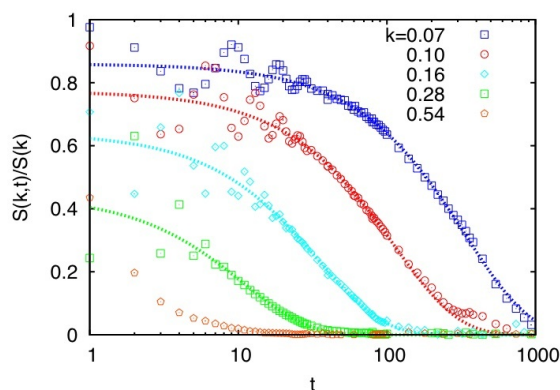


Fig. 8: Normalized intermediate scattering function $S(k,t)/S(k)$ in the hexatic phase at $T = 1.15$ for various small k . After the initial acoustic damped oscillation, it can be fitted to the exponential decay of the form $A_k e^{-\Gamma_k t}$ (solid lines) with $\Gamma_k \propto k^{2.6}$.

Summary and Comments. — We have examined the heterogeneities in structure and dynamics at two-dimensional melting of one-component systems at fixed volume V . In terms of the disorder variable D_j , structurally heterogeneous patterns have emerged unambiguously among the crystalline and disordered regions in the hexatic phase in figs. 2 and 3. Though very weak, we have noticed the presence of large-scale density fluctuations. As a result, at small wave number k , the structure factor $S_6(k)$ of the sixfold orientation order grows strongly as in fig. 4 (a), while the structure factor $S(k)$ of the density grows similarly but its amplitude is very small as in fig. 4 (b). Dynamically heterogeneous patterns have been obtained in fig. 7 in the crystal and hexatic phases. Crystal states are dynamically heterogeneous on long time scales due to relatively rapid motions of defect clusters. In the hexatic phase, dynamics is heterogeneous on short time scales, where the particles with high D_j tend to be mobile than those with small D_j . We have also calculated the intermediate scattering function $S(k,t)$, which has turned out to relax exponentially with the dynamic exponent z about 2.6 at small k in the hexatic phase.

We make further comments. (i) In our simulation, mesoscopic coexistence of the ordered and disordered regions is realized dynamically in the hexatic phase. There are no sharp boundaries between the two regions and the free energy penalty due to the structural inhomogeneity should be very small. These structural fluctuations resemble the critical fluctuations in Ising systems. It remains puzzling whether or not the long wavelength limit of $S(k)$ tends to a finite constant in the thermodynamic limit. If so, it follows a finite compressibility. (ii) Growth (shrinkage) of the disordered regions gives rise to an increase (a decrease) in the pressure p at fixed volume. We should perform constant-pressure simulations also to examine whether or not the hexatic phase exists depends on the boundary condition.

(iii) In binary mixtures the size dispersity serves to pin the particle motions and the relaxation times are much longer than in one-component systems. (iv) Shear flow has been applied to glassy and polycrystal systems [24–26]. It is intriguing how applying shear can affect the hexatic state and the scenario of the 2D melting.

* * *

We thank T. Hamanaka, N. Ito, T. Uneyama, R. Yamamoto, S. Yukawa, H. Watanabe, R. Okamoto, and T. Kawasaki for valuable discussions. This work was supported in part by Grant-in-Aid for Scientific Research on the Priority Area “Soft Matter Physics” and for the Global COE Program “The Next Generation of Physics, Spun from Universality and Emergence” from the MEXT of Japan. H. S. was supported by JSPS.

REFERENCES

- [1] B.J. Alder and T.E. Wainwright, Phys. Rev. **127**, 359 (1962).
- [2] K.J. Strandburg, Rev. Mod. Phys. **60**, 161 (1988).
- [3] F.F. Abraham, Phys. Rep. **80**, 339 (1981).
- [4] S. Toxvaerd, Phys. Rev. A **24**, 2735 (1981).
- [5] H. Weber, D. Marx, and K. Binder, Phys. Rev. B **51**, 14636 (1995).
- [6] B.I. Halperin and D.R. Nelson, Phys. Rev. Lett. **41**, 121 (1978).
- [7] A.H. Marcus and S.A. Rice, Phys. Rev. E **55**, 637 (1997).
- [8] K. Zahn, R. Lenke, and G. Maret, Phys. Rev. Lett. **82**, 2721 (1999).
- [9] K. Zahn and G. Maret, Phys. Rev. Lett. **85**, 3656 (2000).
- [10] R.A. Quinn and J. Goree, Phys. Rev. E **64**, 051404 (2001).
- [11] D.E. Angelescu *et al.*, Phys. Rev. Lett. **95**, 025702 (2005).
- [12] Y. Han *et al.*, Phys. Rev. E **77**, 041406 (2008).
- [13] C. Reichhardt and C. J. O. Reichhardt, Phys. Rev. Lett. **90**, 095504 (2003).
- [14] R. Zangi and S. A. Rice, Phys. Rev. Lett. **92**, 035502 (2004).
- [15] Y. Saito, Phys. Rev. B **26**, 6239 (1982).
- [16] C. Dink and J. van der Elksen, Phys. Rev. B **35**, 279 (1987).
- [17] A. Jaster, Phys. Rev. E **59**, 2594 (1999).
- [18] S. Sengupta, P. Nielaba, and K. Binder, Phys. Rev. E **61**, 6294 (2000).
- [19] H. Watanabe *et al.*, Phys. Rev. E **69**, 045103(R) (2004).
- [20] C.H. Mak, Phys. Rev. E **73**, 065104(R) (2006).
- [21] S.T. Chui, Phys. Rev. B, **28**, 178 (1983).
- [22] M.M. Hurley and P. Harrowell, Phys. Rev. E **52**, 1694 (1995).
- [23] T. Hamanaka and A. Onuki, Phys. Rev. E **74**, 011506 (2006); *ibid.* **75**, 041503 (2007).
- [24] R. Yamamoto and A. Onuki, J. Phys. Soc. Jpn. **66**, 2545 (1997); Phys. Rev. E **58**, 3515 (1998).
- [25] T. Hamanaka, H. Shiba, and A. Onuki, Phys. Rev. E **77**, 042501 (2008).
- [26] A. Onuki, *Phase Transition Dynamics* (Cambridge University Press, Cambridge, 2002).